Journal of Solid State Chemistry **167,** 237–244 (2002)
doi:10.1006/jssc.2002.9650

Structure Determination of the Layered Manganocuprates $Ln_3Ba_2Mn_2Cu_2O_{12\pm y}$, Ln=Sm, Eu, by Powder Neutron Diffraction

M. A. L. Field, C. S. Knee, and M. T. Weller[1]

Department of Chemistry, University of Southampton, Highfield, Southampton, SO17 1BJ, United Kingdom

Received December 12, 2001; in revised form April 9, 2002; accepted May 10, 2002

Samples of $Ln_3Ba_2Mn_2Cu_2O_{12\pm y}$, Ln = Sm, Eu, have been synthesized with non-absorbing isotopes and studied by high-resolution powder neutron diffraction. For Ln = Eu, the material was studied before and after annealing in oxygen. Results show that segregation of the manganese and copper between the layer sites is incomplete and that oxygen can also be incorporated between the CuO_5 square-based pyramids giving the overall composition $Ln_3Ba_2Mn_2Cu_2O_{12.1}$. Cation size mismatch on the *A*-type cation sites leads to a local distortion in the oxide sublattice in the MnO_6 octahedra and consideration of the *A*-site coordination geometries permits an understanding of the limited lanthanide range for which this structure forms. While the *Ln* and Ba cations are fully segregated the observed *B* cation disorder and additional inter-cuprate layer oxygen are likely to preclude observation of superconductivity in this family of materials.

Key Words: **cuprate; manganate; neutron diffraction.**

INTRODUCTION

The oxide chemistries of copper and manganese have recently commanded considerable attention due to the unusual electronic and magnetic properties exhibited by such materials. Much of this attention has been directed at the two specific oxidation states Cu II and Mn III which are Jahn–Teller ions (d^9 and d^4, respectively). In terms of Cu II chemistry, the main thrust has been the synthesis of new high-temperature superconducting compounds constructed from layers of corner-sharing CuO_4 square planes of the formal stoichiometry CuO_2 (1). The structures of these materials are all formally derived from the perovskite structure with various other layers interposed. These inter-cuprate sheets may be of other structure types, such as fluorite or rocksalt, but may also be perovskite based themselves as, for example, materials of the type $Gd_2Ba_2Ti_2Cu_2O_{12}$ (2). With respect to Mn III chemistry, the aim has been the formation of mixed valency Mn III/Mn IV materials demonstrating magnetoresistance properties such as $Ln_{1-x}Ca_xMnO_3$ (3) and $LaSr_2Mn_2O_7$ (4). Again these structures are based on perovskites though, unlike superconductor chemistry, a three-dimensional component to the structure seems to be required for the observation of the property of interest.

The combination of manganese and copper in complex perovskite-based structures has been achieved by Hervieu *et al.* (5) and studied in detail by Matsubara and co-workers (6–8). Materials of the composition $Ln_3Ba_2Mn_2Cu_2O_{12}$ exist only for Ln = Sm, Eu, Gd and adopt the so-called intergrowth structure between 123 and 0201, i.e., a perovskite–rocksalt intergrowth. The structure, shown in Fig. 1, has K_2NiF_4 layers of the composition Ln_2MnO_4 alternating with 123 layers of the formal composition $LnBa_2Cu_2MnO_8$. For an overall oxygen stoichiometry of $y=0$ in the formula $Ln_3Ba_2Mn_2Cu_2O_{12\pm y}$, this produces a mixed Mn III/IV material with a manganese oxidation state typical of that observed in GMR materials. Cation substitutions have also been performed on this system forming, for example, $(Eu_{3-x}Ca_x)Ba_2Mn_{2-y}Sc_yCu_2O_{12}$ with the aim of formally oxidizing copper into the superconducting regime around $Cu^{2.25+}$ but all such phases were found to be semiconducting (8).

All the structural analyses carried out on members of the $Ln_3Ba_2Mn_2Cu_2O_{12\pm y}$ so far have used powder X-ray diffraction methods or electron microscopy. Such techniques are relatively insensitive to oxygen distributions due to the presence of the heavier, strongly scattering elements. In addition, the similarity of manganese and copper and of lanthanide and barium ions in terms of the scattering of X-rays makes distinguishing these elements extremely difficult. In order to rationalise the properties of the members of the $Ln_3Ba_2Mn_2Cu_2O_{12\pm y}$ system, determinations of the distributions and levels of oxygen and the

[1]To whom correspondence should be addressed. Fax: +023-80596805. E-mail: mtw@soton.ac.uk.

0022-4596/02 $35.00

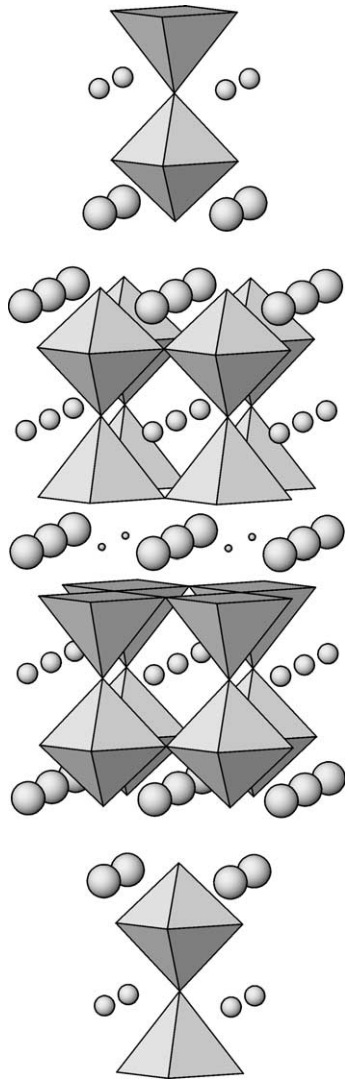

FIG. 1. Idealized $Ln_3Ba_2Mn_2Cu_2O_{12}$ structure showing CuO_5 square-based pyramids and MnO_6 octahedra. *Ln*: large spheres; Ba: medium spheres.

cations on their respective sub-lattices are obviously crucial. The technique of choice for such a study is powder neutron diffraction where oxygen is a strong neutron scatterer and significant scattering contrasts can exist between near-neighbor elements; e.g., Mn $b = -3.7$ fm, Cu $b = 7.7$ fm. However, the small range of lanthanides for which the $Ln_3Ba_2Mn_2Cu_2O_{12\pm y}$ phase forms normally precludes the use of neutron diffraction methods as naturally occurring isotopic composition Gd, Sm and Eu are all strong neutron absorbers. This problem may be overcome through the use of specific lanthanide isotopes which are only weakly absorbing such as ^{160}Gd, ^{154}Sm and ^{153}Eu. In this work, we report the structural study of $^{154}Sm_3Ba_2Mn_2Cu_2O_{12\pm y}$ and $^{153}Eu_3Ba_2Mn_2Cu_2O_{12\pm y}$, in as-prepared and oxygen-annealed forms, by high-resolution neutron diffraction.

EXPERIMENTAL

Samples of $Ln_3Ba_2Mn_2Cu_2O_{12}$ ($Ln = {}^{153}$Eu, ^{154}Sm) were prepared by conventional solid-state reactions of Ln_2O_3 ($Ln = {}^{153}$Eu, ^{154}Sm), $BaCO_3$, Mn_2O_3 and CuO (all 99.9% or better) in platinum crucibles. Approximately 1 g of each material was synthesized. The lanthanide isotopes were purchased from Trace Isotope at a level of > 98.7% purity. These reactants were well ground to form an intimate mixture and formed into pellets under 10 ton/cm^2 before firing at 1000°C for 4 h and at 1100°C for 4 h with an intermediate grinding and pelletizing. Three further treatments at 1100°C improved phase purity in both samples. Powder X-ray diffraction data collected on a Siemens D5000 diffractometer operating with Cu$K\alpha_1$ radiation showed good phase purity for the europium-based target phase with impurity lines having $I/I_0 < 2\%$. The synthesis of pure $Sm_3Ba_2Mn_2Cu_2O_{12}$ proved more difficult, possibly as the larger lanthanide is of a poorer match for the ordered layered structure, *vide infra*, and the level of $Sm_2BaCuMnO_7$ remained close to 20% in the product.

A portion of the $^{153}Eu_3Ba_2Mn_2Cu_2O_{12}$ sample also underwent an overnight anneal in oxygen at 1050°C, with slow cooling in oxygen to room temperature, after collection of the initial neutron diffraction data set. Powder X-ray diffraction data of this annealed product showed a small increase in *c* lattice parameter in comparison with the as-prepared material.

Neutron powder diffraction data were collected from 500 mg–1 g samples on the HRPD at Rutherford Appleton Laboratories at 298, 150 and 2 K for the $^{153}Eu_3Ba_2Mn_2Cu_2O_{12}$ sample and 298 K only for the $^{154}Sm_3Ba_2Mn_2Cu_2O_{12}$ and oxygen-annealed, 500 mg sample, $^{153}Eu_3Ba_2Mn_2Cu_2O_{12}$ samples. Data collection times were 16 h and data reduction was carried out using the standard methods; both back-scattering and 90° data banks were included in the structure refinement which employed the GSAS package (9). Raw data from the europium-containing samples were corrected for the effects of absorption due to the residual ^{151}Eu in the sample. For the samarium-based material, such data correction proved more difficult, due to the presence of the secondary phase, and an absorption correction was not undertaken for this data set.

STRUCTURE REFINEMENT STRATEGY

The model used as the basis for the refinements was that given by Hervieu *et al.* (5). Initially, the room temperature data set from $^{153}Eu_3Ba_2Mn_2Cu_2O_{12}$ was analyzed; identical methodology was subsequently employed for the data collected at the lower temperatures and from the oxygen-annealed and samarium samples. The tetragonal unit cell, 3.88×35.2 Å, could account for all the reflections in the diffraction profiles of the europium-based phases except

for a few weak peaks that could be discerned in the 90° bank data set; for $^{154}Sm_3Ba_2Mn_2Cu_2O_{12}$, few moderate intensity reflections demanded the incorporation of $Sm_2BaCuMnO_7$ as a second phase in the refinement. For these data, no absorption coefficient was refined leading to negative thermal displacement parameters for the absorbing atom positions due to strong correlations in these two parameters. Scattering lengths were taken as default values within GSAS except for ^{154}Sm, 9.30 fm, and ^{153}Eu, 8.22 fm.

In the initial stages of the refinement, the manganese was placed solely on the (0,0,0.16) position and copper on the (0,0,0.04) site; oxygen atoms were confined to the special sites as given by Hervieu *et al.* (5). The refinement proceeded satisfactorily with incorporation of instrument parameters, atomic positions and atomic displacement parameters. Inspection of the refined atomic displacement parameters showed a number of anomalies. The values for the manganese and copper sites became unrealistically large, $100 \times U_{iso} > 8\text{Å}^2$, indicating that for both sites the scattering was of a lower magnitude. The displacement parameters for O(4) (near (0,0,0.22) and forming an apex to the MnO_6 octahedron) were significantly higher than those for the other oxygen sites within the material. The structural model was therefore modified by allowing copper and manganese to distribute over the two (0,0,z) sites. Initially, the site occupancies were allowed to vary freely but the 1:1 overall Cu:Mn ratio was retained within e.s.d.' so this composition was fixed over the two sites for the remainder of the refinement. In order to maintain stability in the refinement, the thermal displacement parameters of the two sites and each of the two atoms occupying them were constrained to be equal though this value was allowed to vary. Such a constraint can be crucial as partially replacing manganese ($b = -3.73$ fm) by copper ($b = 7.718$ fm) can lead to a small effective scattering from a site, making determination of its thermal displacement parameter impossible. Refinement of anisotropic thermal displacement parameters for O(4) demonstrated the origin of the high U_{iso} for this site with large components found in the xy plane. This is a manifestation of disorder in the oxygen position in this plane as has been observed in other layered perovskites where there is mismatch between the various A and B cation types and their coordination to oxygen. Therefore, this oxygen was displaced onto an (x,0,z) site with $x \approx 0.1$ and $z \approx 0.22$ with $\frac{1}{4}$ occupancy and both positional parameters and the isotropic thermal displacement parameter varied; the refinement converged smoothly on this basis. Inspection of the barium and lanthanide atom displacement parameters showed these values to be reasonable and attempts to disorder these ions reverted to the perfect segregation proposed by Hervieu *et al.* (5) which was, therefore, maintained in the final stages of the refinement.

One further aspect of the oxygen distribution was probed in the final stages of the refinement. The $(\frac{1}{2},\frac{1}{2},\frac{1}{2})$ site, which lies between the CuO_5 square pyramids, is formally vacant in the basic structural model. However, given the partial displacement of manganese onto this site, refined here, it is possible that partial occupancy of this "inter-cuprate" layer site occurs. Therefore, oxygen was allowed to occupy the $(\frac{1}{2},\frac{1}{2},\frac{1}{2})$ site and its occupancy factor was refined, leading to a small, but statistically significant determined site occupation. Refinement of both the small occupation factor and thermal displacement parameter for this site proved problematical so they were refined in alternate cycles. The final refined stoichiometry was equivalent to $^{153}Eu_3Ba_2Mn_2Cu_2O_{12.1}$.

The overall profile fit to the back-scattering data was excellent, but close inspection of the 90° bank data at longer d-spacings showed a few weak additional reflections not fitted by the $^{153}Eu_3Ba_2Mn_2Cu_2O_{12.1}$ unit cell. A number of these could be assigned to the cryostat and aluminum but three further reflections could not be allocated to such instrumental origins. The d-spacings of these reflections lying to slightly larger d-spacings than the main reflections from the $^{153}Eu_3Ba_2Mn_2Cu_2O_{12.1}$ phase could be assigned to a perovskite-like impurity and a reasonable fit could be achieved using an orthorhombic $GdFeO_3$-type structure as, for example, adopted by compositionally similar Gd_2MnCoO_6 (10). Such a structure type was introduced into the refinement as disordered (Eu,Ba)(Mn,Cu)O_3 and refinement of the lattice parameters and phase fraction alone for this phase produced a slight improvement to the profile fit. However, given the paucity of data, three fairly weak reflections, full refinement of this additional phase was not attempted; the refinement of the phase fraction indicated a weight fraction within the sample of $< 5\%$. It can be seen from Fig. 2 that one region of the profiles, centered around 2.15 Å, was excluded from the final refinements; this excluded region contains scattering from the cryostat.

A similar refinement process was followed for each of the other three data sets from $^{153}Eu_3Ba_2Mn_2Cu_2O_{12+y}$, and in each case convergence was reached. Refined atomic coordinates, lattice parameters, profile fit factors and derived bond lengths and angles are summarized in Table 1. Table 2 summarizes the derived bond lengths and angles of importance and Fig. 2 shows a typical profile fit as obtained to $^{153}Eu_3Ba_2Mn_2Cu_2O_{12+y}$ 150 K data. For $^{154}Sm_3Ba_2Mn_2Cu_2O_{12+y}$, a similar refinement methodology was used but with the incorporation of $Sm_2BaCuMnO_7$ as a second phase in the refinement process and the use of excluded regions to remove peaks deriving from instrumental factors. A coordinate description for $Sm_2BaCuMnO_7$ was taken from the well-known Ruddlesden–Popper phase $Sr_3Ti_2O_7$ (11) with fully disordered A and B cation sites, and only the basic

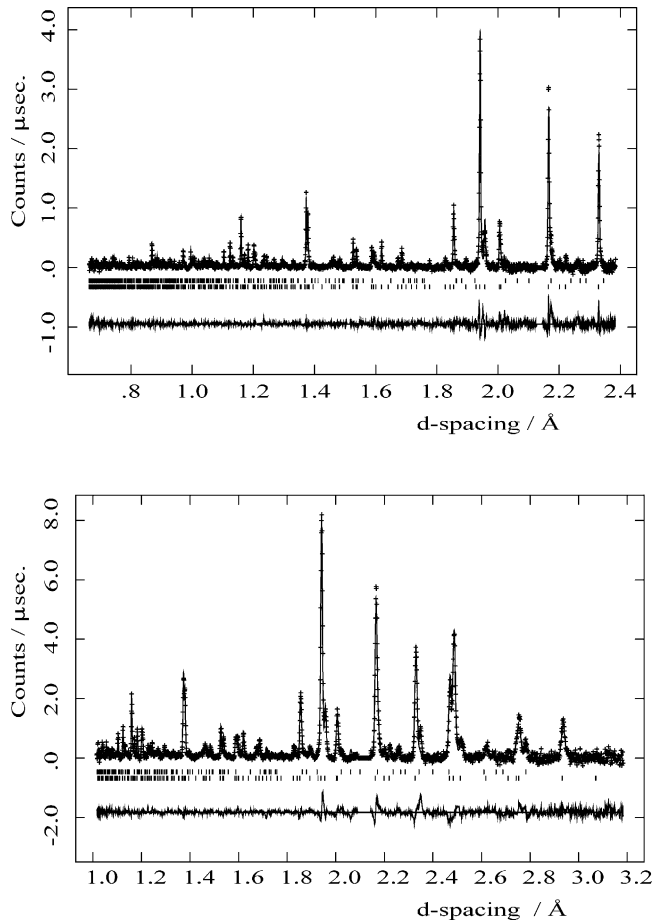

FIG. 2. Final profile fit achieved to the powder neutron diffraction data from $Eu_3Ba_2Mn_2Cu_2O_{12.1}$ at 150 K. Cross marks are observed data, upper continuous line the calculated profile and lower the difference. Tick marks give the reflection positions, lower set for $Eu_3Ba_2Mn_2Cu_2O_{12.1}$ and upper set for (Eu,Ba)(Mn,Cu)O_3.

instrumental and structural parameters refined in order to fit the contribution of this phase to the profile. For sites occupied by samarium, the thermal displacement factors refined to significant negative values; this is an artifact of the sample absorption, not corrected for in this sample but significant for the presence of $\sim 1\%$ ^{149}Sm (absorption cross section 42,080 b) Figs. 3 and 4.

Bond valence calculations following the method of Altermatt and Brown (12) for the cation sites in $^{153}Eu_3Ba_2Mn_2Cu_2O_{12+y}$ at 298 K are summarized in Table 3.

DISCUSSION

The idealized $Ln_3Ba_2Mn_2Cu_2O_{12}$ structure is shown in Fig. 1 and consists of a K_2NiF_4 structure block formally based on manganese separated by 123-type blocks based on copper. Alternatively, the structure can be considered as an oxygen-deficient quadruple perovskite block with the layer sequence MnO_6–CuO_5–CuO_5–MnO_6 separated by rocksalt layers based on EuO; full oxygen occupancy of the perovskite layers would give a stoichiometry of the type $A_5B_4O_{13}$, which is the $n=4$ member of the Ruddlesden–Popper series $A_{n+1}B_nO_{3n+1}$.

However, as with many mixed A and B cation perovskite superstructures, the true structure is more complex as each of the cation types has specific structural and coordinative requirements that cannot all necessarily be satisfied. In addition there exists, for systems containing more than one A or B cation type, the potential for ordered, partially ordered or fully disordered distributions.

In $Eu_3Ba_2Mn_2Cu_2O_{12.1}$, there is a significant mixing between the formally copper and manganese sites. In each sample studied, this mixing was refined independently at $0.83(\pm 0.05)/0.17$, confirming unequivocally that, in this structure, full segregation of the B cation types does not occur. The presence of a small level of impurity ($\sim 3\%$) of the type (Eu,Ba)(Mn,Cu)O_3 in the product has little influence on the stoichiometry of the main phase; the presence of this material, also with a perovskite-based structure and similar unit-cell parameters, only becomes apparent under very high-resolution neutron diffraction. Presumably, this phase represents a greater degree of manganese and copper disordering than is seen in $Eu_3Ba_2Mn_2Cu_2O_{12.1}$ and its observation may be related to the presence of intergrowths phases as observed by Hervieu *et al.* (5).

For double perovskites of the type $AA'BB'O_n$, Anderson *et al.* (13) have defined rules controlling whether two B cations will separate into ordered structures, either layered or three dimensional. This includes the requirement for large charge differences on B and B' (the charge on B' two higher than that on B), ionic size differences (B' larger than B) and additional structure directing parameters, such as the Jahn–Teller effect, to promote layering of the two ions. Consideration of $Mn^{3+/4+}$ and Cu^{2+} as present in $Eu_3Ba_2Mn_2Cu_2O_{12.1}$ indicates that there is a driving force for segregation of these ion types but it is equivocal. The formal charge difference is 1.5+, the ionic radii r (Mn^{3+}) $=0.58$ Å, r (Mn^{4+}) $=0.53$ Å and r (Cu^{2+}) $=0.60$ Å (as modified and used in Ref. (13)) and both Mn^{3+} and Cu^{2+} are subject to Jahn–Teller distortions. These data should be compared with tin (IV), r (Sn^{4+}) $=0.69$ Å, which layers with Cu^{2+} in La_2SnCuO_6 (13). So while Mn^{4+} and Cu^{2+} would be expected to have tendencies towards ordering, the same would not be expected of Mn^{3+} and Cu^{2+}. Hence, the observed incomplete separation of manganese and copper in $Eu_3Ba_2Mn_2Cu_2O_{12.1}$ is consistent with these arguments with a tendency of manganese, presumably as Mn^{3+}, to disorder onto the copper site. Bond valence calculations for manganese and copper support the refined coordination geometries (Table 3), with calculations based on Cu^{2+} producing a bond valence sum of 2.1 and both

TABLE 1
Refined Atomic Coordinates, Lattice Parameters, and Profile Fit Factors

	Eu as-prepared, 2 K	Eu as-prepared, 150 K	Eu as-prepared, 298 K	Eu O_2-annealed	Sm as-prepared, 298 K
U_{iso} Eu/Sm(1)	−0.06(6)	0.06 (7)	0.69(7)	0.82(5)	−1.28(9)
$z_{Eu/Sm(2)}$	0.71209(5)	0.71206(6)	0.71211(6)	0.71212(4)	0.71225(6)
U_{iso} Eu/Sm(2)	0.75(5)	0.87(6)	1.58(6)	1.70(4)	−0.35(7)
z_{Ba}	0.60459(8)	0.60472(10)	0.60516(10)	0.60560(7)	0.60462(12)
U_{iso} Ba	0.78(5)	0.96(6)	1.12(7)	1.27(5)	3.09(12)
z_{Cu}	0.04790(7)	0.04790(8)	0.04799(8)	0.04798(6)	0.04853(11)
n_{Cu}	0.836(3)	0.830(4)	0.837(4)	0.818(2)	0.803(4)
U_{iso} Cu/Mn	0.21(6)	0.27(7)	0.50(8)	0.64(5)	1.80(11)
z_{Mn}	0.1649(2)	0.1646(3)	0.1645(3)	0.1649(2)	0.1654(4)
$z_{O(1)}$	0.04250(5)	0.04240(6)	0.04227(6)	0.04225(4)	0.04306(6)
U_{iso} O(1)	1.21(4)	1.38(5)	1.52(5)	1.57(5)	2.69(7)
$z_{O(2)}$	0.11305(8)	0.11309(9)	0.11302(9)	0.11312(6)	0.11344(11)
U_{iso} O(2)	1.72(7)	1.84(8)	1.99(8)	1.98(4)	3.41(11)
$z_{O(3)}$	0.17124(5)	0.17124(6)	0.17116(6)	0.17090(4)	0.16976(8)
U_{iso} O(3)	1.87(4)	1.97(5)	2.19(5)	2.30(3)	3.50(7)
$x_{O(4)}$	0.0899(11)	0.0868(13)	0.0806(17)	0.0736(15)	0.0834(14)
$z_{O(4)}$	0.22348(9)	0.22354(10)	0.22385(11)	0.22375(7)	0.22270(12)
U_{iso} O(4)	0.36(13)	0.57(16)	1.13(18)	2.18(14)	3.52(8)
$n_{O(5)}$	0.108(10)	0.091(11)	0.091(12)	0.122(7)	0.150(12)
U_{iso} O(5)	1.3(1.0)	1.4(1.2)	1.7(1.4)	2.0(8)	3.5(1.0)
a/Å	3.88081(2)	3.88176(2)	3.88500(2)	3.88136(2)	3.88362(3)
c/Å	35.1795(3)	35.2197(4)	35.2949(4)	35.3507(3)	35.4928(5)
R_p	2.44	2.48	2.71	9.53	6.89
R_{wp}	4.24	4.26	4.75	11.9	7.45
R_{exp}	2.44	3.12	3.02	6.43	3.10
χ^2	3.01	1.86	2.48	3.43	5.79

Note. Space group $I4/mmm$ Eu/Sm(1) on $\left(0,0,\frac{1}{2}\right)$, Eu/Sm(2) on $(0,0,z_{Eu/Sm(2)})$, Ba on $(0,0,z_{Ba})$, Cu(Mn) on $(0,0,z_{Cu})$ with Cu site occupancy residual is n_{Mn} $(1-n_{Cu})$, Mn(Cu) on $(0,0,z_{Mn})$ with Mn site occupancy $n_{Mn,}$ O(1) on $(\frac{1}{2}, 0, z_{O(1)})$, O(2) on $(0,0,z_{O(2)})$, O(3) on $(\frac{1}{2},0,z_{O(3)})$, O(4) on $(x_{O(4)},0,z_{O(4)})$ with $\frac{1}{4}$ occupancy, O(5) on $\left(\frac{1}{2},\frac{1}{2},\frac{1}{2}\right)$ with site occupancy $n_{O(5)}$. Thermal displacement parameters (all $\times 100$, (Å^2)) for each atom site are also given; values for Cu and Mn were constrained to be equal.

TABLE 2
Derived Bond Lengths and Angles of Note

Bond	Eu as-prepared, 2 K	Eu as-prepared, 150 K	Eu as-prepared, 298 K	Eu O_2-annealed, 298 K	Sm as-prepared, 298 K
Eu(1)–O(1) × 8	2.450(1)	2.449(1)	2.449(1)	2.449(1)	2.471(1)
Eu(1)–O(5) × 4[a]	2.7442(1)	2.7448(1)	2.7471(1)	2.7445(1)	2.7461(1)
Eu(2)–O(3) × 4	2.415(2)	2.415(2)	2.421(2)	2.427(1)	2.459(2)
Eu(2)–O(4a) × 2[a]	3.027(3)	3.020(4)	3.005(5)	2.982(4)	3.007(4)
× 2[a]	2.541(3)	2.550(3)	2.569(4)	2.583(4)	2.554(4)
Eu(2)–O(4b) × 1[a]	2.293(4)	2.293(5)	2.282(5)	2.285(3)	2.332(5)
Ba–O(1) × 4	2.922(3)	2.930(3)	2.950(4)	2.964(2)	2.924(4)
Ba–O(2) × 4	2.7602(4)	2.7606(5)	2.7611(5)	2.7574(1)	2.7638(6)
Ba–O(3) × 4	3.044(3)	3.042(3)	3.033(4)	3.016(2)	3.019(4)
Cu(Mn)–O(1) × 4	1.9497(3)	1.9505(3)	1.9530(4)	1.9512(3)	1.9515(4)
Cu(Mn)–O(2) × 1	2.292(4)	2.296(4)	2.295(4)	2.303(3)	2.304(5)
Cu(Mn)–O(5) × 1[a]	1.685(2)	1.687(3)	1.694(3)	1.696(2)	1.722(4)
Mn(Cu)–O(2) × 1	1.825(9)	1.815(10)	1.817(10)	1.830(7)	1.838(15)
Mn(Cu)–O(3) × 4	1.9531(9)	1.9548(12)	1.9566(12)	1.9523(8)	1.9484(11)
Mn(Cu)–O(4b) × 1[a]	2.089(8)	2.103(9)	2.118(9)	2.100(7)	2.064(14)
O(4) off-axis displacement	9.62(12)	9.23(15)	8.5(2)	7.82(15)	9.1(2)
Cu–O(1)–Cu	168.8(2)	168.6(2)	168.1(1)	168.1(2)	168.6(2)
Mn–O(3)–Mn	166.9(5)	166.3(6)	166.2(6)	167.5(4)	171.0(9)

[a] Indicates partially occupied site.

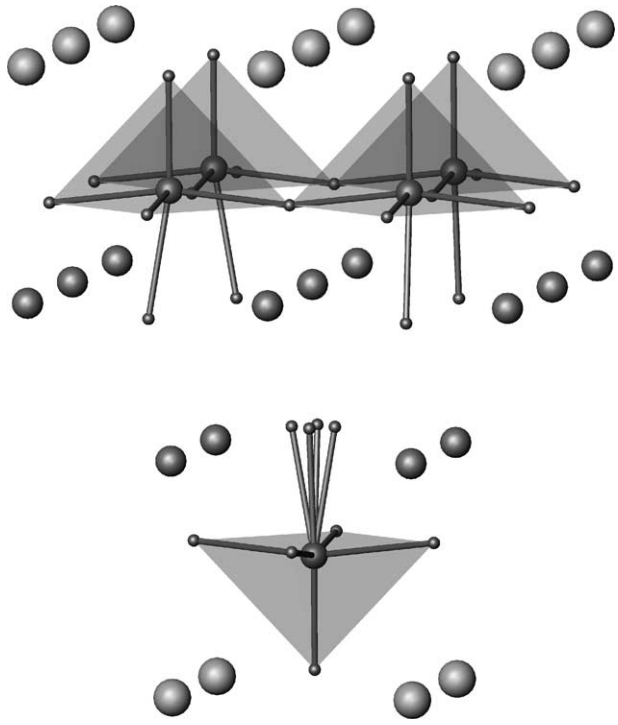

FIG. 3. Section of the $Eu_3Ba_2Mn_2Cu_2O_{12}$ structure showing the local displacements of O(4) and coordination to Eu. For the lower CuO_5 square pyramid, all positions are shown, for the upper layer a possible local arrangement of O(4) over the disordered site is reproduced.

Mn^{3+} and Mn^{4+} values giving manganese bond valence sums close to 3.5.

In $Eu_3Ba_2Mn_2Cu_2O_{12.1}$, the Eu^{3+} and Ba^{2+} cations are fully ordered presumably as a result of significant differences in ion size (r (Eu^{3+}) = 1.07 Å and r (Ba^{2+}) = 1.42 Å,

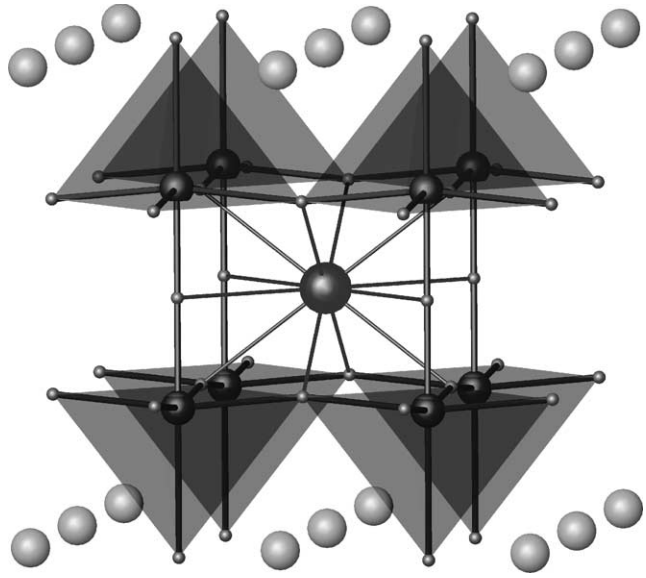

FIG. 4. Section of the $Eu_3Ba_2Mn_2Cu_2O_{12}$ structure showing the partially occupied O(5) $\left(\frac{1}{2},\frac{1}{2},\frac{1}{2}\right)$ site.

in eight-fold coordination) and coordination preferences. Europium adopts the lower eight and nine coordination sites to oxygen while barium is 12 coordinated (r (Ba^{2+}) = 1.61 Å in 12-fold coordination).

The further consequence of layering *B*-type cations in perovskite-type structures is mismatch in the sheet dimensions which leads to buckling of layers and rotation of the polyhedra as is seen, for example, in $Ln_2Ba_2Ti_2Cu_2O_{12}$ (14) and $GdSr_2RuCu_2O_8$ (15). These oxygen atom shifts which occur may also be associated with the coordination preferences of the *A*-type cations, which are better served through local and long-range displacements of the oxygen atoms. In $Eu_3Ba_2Mn_2Cu_2O_{12.1}$, these oxygen displacements are associated with O(4), the terminal oxygen of the MnO_6 octahedra in the Eu_2O_2 layers, and are probably a result of coordination preferences of Eu and the otherwise weak interaction of this oxygen with the cations. Without displacements, the Eu–O distances would be $4 \times 2.421 + 4 \times 2.773 + 1 \times 2.265$ Å though following the local displacements this later four become, on average, $2 \times 2.569 + 2 \times 3.005$ Å. In terms of bond valence calculations, this has the effect of increasing the Eu bond valence to 2.82 from 2.77; see Table 3. For the oxygen itself, bond valence calculations give values well below 2 which are increased slightly through the local displacement towards europium.

The final feature of interest in the $Eu_3Ba_2Mn_2Cu_2O_{12.1}$ structure is the partial occupancy of the $\left(\frac{1}{2},\frac{1}{2},\frac{1}{2}\right)$ site by oxygen. The refined value of 0.10(1) is significant and was refined independently for each data set. It is likely that occupation of this site is associated with the partial occupation of the neighboring site by manganese. Intriguingly, the refined occupancy for this site, which bridges two square-based CuO_5 pyramids, is almost exactly half the level of manganese substitution on this square pyramidal site. It is therefore tempting to conclude that the manganese may locally order in the structure replacing $O_5Cu..\square..CuO_5$, where $\square$ represents the vacant $\left(\frac{1}{2},\frac{1}{2},\frac{1}{2}\right)$ position, by $O_5Mn..O..MnO_5$ in 10% of site pairs. Local, more extensive, disordering of these cations could be the origin of the formation of the $(Eu,Ba)(Mn,Cu)O_3$-type structure.

For the samarium derivative the main differences are those expected as a result of replacing europium (r (Eu^{3+}) = 1.07 Å) by the larger samarium (r (Sm^{3+}) = 1.08 Å); the presence of a higher level of impurity for this product merits caution in interpreting the results in terms of the cation composition though extracted distances and angles have equal validity. Both the a and c lattice parameters increase as do the average bond lengths around the lanthanide site resulting in a reduced buckling on the MnO_2 layers (Mn–O–Mn increasing from 167° to 171°); the local environments of the barium and Mn/Cu are largely unaffected. More important are the differences in

TABLE 3
Bond Valence Sums for $Eu_3Ba_2Mn_2Cu_2O_{12}$ at 298 K (the Number of Each Bond Is Given in Table 2)

Atom	Eu(1)	Eu(2), 4 × O(4)	Eu(2), 2 × O(4a), 2 × O(4a′)	Ba	Cu II	Cu III	Mn III	Mn IV	Oxygen valence
O(1)	0.3630	—	—	0.1657	0.4769	0.5608	—	—	**2.01** Cu II
O(2)	—	—	—	0.2762	0.1892	0.2225	0.8572	0.8412	**2.15** Cu II
O(3)	—	0.3915	0.3915	0.1324	—	—	0.5878	0.5768	**2.22** Mn III
O(4*a*)	—	0.1512 (a)	0.2624 (b) 0.0808 (b)	—	—	—	—	—	**1.58** (a) Mn III
O(4*b*)	—	0.5968 (a)	0.5700 (b)	—	—	—	0.3800	0.3729	**1.64** (b) Mn III
O(5) × 0.1	0.1622	—	—	—	n/a	n/a	—	—	—
Cation valence	**2.97**	**2.78**	**2.82**	**2.30**	**2.10**	**2.47**	**3.59**	**3.52**	—

Note. The values marked as (a) and (b) differentiate the two europium–oxygen bonding models based on O(4) on special site (a) and displaced onto (x,0,z) (b) leading to different bond valence sums.

some of the associated structural features in that (i) there is a small increase in the distortion around the lanthanide site and (ii) the oxygen level on the partially occupied site adjacent to the lanthanide is significantly higher for samarium. This latter factor seems to be mainly a result in the change in size of the lanthanide ion rather than a significant increase in the level of manganese on the copper site, which is marginally higher at 0.19 (cf 0.17 for Eu). Clearly, placing the samarium between the cuprate layers increases their separation, as a result of the increased Ln – O(1) distance, Cu···Cu is 3.388 Å at 298 K for Ln = Eu in $Ln_3Ba_2Mn_2Cu_2O_{12}$ but 3.434 Å for Ln = Sm and thus oxygen can more easily occupy this site.

The limits in terms of lanthanide size that exist for the $Ln_3Ba_2Mn_2Cu_2O_{12}$ series can be rationalized in terms of the structure presented here. For lanthanides larger than Sm, formation of this phase is difficult and the origin of this behavior resides in the Ln(1) site which is formally coordinated to eight oxygen atoms in the idealized structure. However, for the larger lanthanides, the desire to increase their coordination to oxygen in oxides above eight with longer Ln–O distances means that incorporation of oxygen onto the $\left(\frac{1}{2},\frac{1}{2},\frac{1}{2}\right)$ with concomitant displacement of manganese, presumably as Mn^{4+}, onto the neighboring position becomes more facile. The structure therefore moves towards a more disordered arrangement in terms of B cation and oxide ion distributions. The end result is the formation of disordered structures, like the impurity phase $Sm_2BaMnCuO_7$, where manganese and copper share a site. For smaller lanthanides, incorporation into the rocksalt layers presumably becomes unfavorable as is illustrated by the existence of the K_2NiF_4 structure for Ln_2CuO_4 only for Ln = La (16) and in distorted form; for Ln_2CuO_4, Ln = Nd–Gd the T′- type structure forms (17).

The effect of oxygen annealing $Ln_3Ba_2Mn_2Cu_2O_{12}$ is small in terms of changes in the structure. A small increase in the manganese occupancy of the copper site occurs (0.182(2) from 0.165(4)) with an associated increase in the occupancy of the partially filled oxygen site O(5) (0.12(1) from 0.10(1)). These changes in cation and oxygen distribution result in small changes in the geometry of the $Cu(Mn)O_5$ square-based pyramid, with a lengthening of the apical bond and a shortening of the in-plane bonds which is reflected in the observed decrease in a parameter and increase in c parameter.

CONCLUSIONS

The $Ln_3Ba_2Mn_2Cu_2O_{12}$ structure is one of the rare complex oxide types which has two B-type cations in perovskite structure elements formally ordered in layers. Similar behavior was first seen for quadruple perovskites containing Sn and Cu (18), and subsequently reported for Ti and Cu (2), Ru and Cu (15) and In and Cu in $Ba_2InCuO_{5+\delta}$ (19), and is a requirement for producing cuprates that might demonstrate superconductivity. More normally, the B cations are fully disordered or form ordered three-dimensional arrays. However, for the $Ln_3Ba_2Mn_2Cu_2O_{12}$ compounds, the B cation ordering has been shown to be imperfect and the displacement of around 15–20% of manganese ions into the CuO_2 sheets is likely to destroy any chance of superconductivity. In addition, the partial cross-linking of $Cu(Mn)O_5$ square pyramids through the addition of excess oxygen will also be an interfering effect. The chances of forming fully segregated copper and manganese sites and eliminating the additional oxygen is highest for smaller lanthanides which will contract the inter-CuO_5 square-pyramid distance and inhibit manganese occupation of these sites. The

smaller lanthanide sizes are not compatible with the ninefold coordination required of this ion in the rocksalt layers.

Clearly, the structure should be stabilized by the introduction of two different cation types and sizes to fit the two types of site occupied by europium in $Eu_3Ba_2Mn_2Cu_2O_{12.1}$. Similar studies have been undertaken on the quadruple and quintuple titanocuprate perovksites with the formation of materials such as $NdDyBa_2Cu_2Ti_2O_{11}$ and $NdDyCaBa_{1.5}Sr_{0.5}Cu_{2.2}Ti_{2.8}O_{14}$ (20–23). However, our attempts to synthesize materials such as $DyNd_2Ba_2Cu_2Mn_2O_{12}$ have been unsuccessful, resulting in the preferred formation of competing phases such as $Ln_2BaMnCuO_7$ and Ln_2CuO_4. Finally, the partial displacement of manganese onto the copper sites permits the formation of some linked MnO_n polyhedra in the *c* direction as well as the *ab* plane, and given, the overall manganese oxidation state near 3.5, these materials could demonstrate magnetoresistive effects.

ACKNOWLEDGMENTS

We thank EPSRC for a studentship for M.A.L.F. and support under grants GR/M21836 and GR/M21188. We also thank R. M. Ibberson and K. S. Knight, Rutherford–Appleton Laboratory for technical assistance.

REFERENCES

1. R. J. Cava, *J. Am. Ceram. Soc.* **83,** 5–28 (2000); J. Karpinski, G. I. Meijer, H. Schwer, R. Molinski, E. Kopnin, K. Conder, M. Angst, J. Jun, S. Kazakov, A. Wisniewski, R. Puzniak, J. Hofer, V. Alyoshin, and A. Sin, *Supercond. Sci. Technol.* **12,** R153 (1999).
2. A. Gormezano and M. T. Weller, *J. Mater. Chem.* **7**(3), 771–772 (1993).
3. J. B. A. A. Elemans, B. van Laar, K. R. van der Veen, and B. O. Loopstra, *J. Solid State Chem.* **3,** 238–242 (1971).
4. P. D. Battle, M. A. Green, N. S. Laskey, J. E. Millburn, M. J. Rosseinsky, S. P. Sullivan, and J. F. Vente, *Chem. Commun.* **6,** 767–768 (1996).
5. M. Hervieu, C. Michel, R. Genouel, A. Maignan, and B. Raveau; *J. Solid State Chem.* **115,** 1–6 (1995).
6. I. Matsubara, N. Kida, R. Funahashi, and K. Ueno, *Chem. Lett.* 971–972 (1996).
7. I. Matsubara, N. Kida, R. Funahashi, K. Ueno, and H. Ishikawa, *Physica C* **282–287,** 945–946 (1997).
8. I. Matsubara, N. Kida, R. Funahashi, K. Ueno, H. Ishikawa, and N. Ohno, *J. Solid State Chem.* **141,** 546-553 (1998).
9. A. C. Larson, R. B. von Dreele, "Generalised Structure Analysis System," Los Alamos National Laboratory, 1994.
10. A. Marsh and C. C. Clark, *Philos. Mag.* **19,** 449 (1969)
11. M. M. Elcombe, E. H. Kisi, K. D. Hawkins, T. J. White, P. Goodman, and S. Matheson, *Acta Crystallogr. B* **47,** 305–314 (1991).
12. D. Altermatt and I. D. Brown, *Acta Crystallogr. B* **41,** 240–244 (1985).
13. M. T. Anderson, K. B. Greenwood, G. A. Taylor, and K. R. Poeppelmeier, *Prog. Solid State Chem.* **22,** 197–233 (1993).
14. M. T. Weller, M. J. Pack, and N. Binsted, *Angew. Chem. Int. Ed.* **37,** 1094–1096 (1998).
15. O. Chmaissem, J. D. Jorgensen, H. Shaked, P. Dollar, and J. L. Tallon. *Phys. Rev. B* **61,** 6401 (2000).
16. P. Zolliker, D. E. Cox, J. B. Parise, E. M. Carron III, and W. E. Farneth. *Phys. Rev. B:* **42,** 6332–6341 (1990).
17. T. Uzumaki, N. Kamehara, and K. Niwa, *Jpn. J. Appl. Phys.* **30**(Part 2), L981–L984 (1991).
18. M. T. Anderson, K. R. Poeppelmeier, *Chem. Mater.* **3**, 476-482 (1991); M. T. Anderson, K. R. Poeppelmeier, J.-P. Zhang, H.-J. Ian, and L. D. Marks, *Chem. Mater.* **4,** 1305–1313 (1992); P. A. Salvador L. Shen, and T. O.Mason, K. B. Greenwood, and K. R. Poeppelmeier, *J. Solid State Chem.* **119,** 80–89 (1995).
19. D. H. Gregory and M. T. Weller, *J. Solid State Chem.* **107,** 134–148 (1993).
20. N. Mansourian-Hadavi, D. Ko, T. O. Mason, and K. R. Poeppelmeier, *J. Solid State Chem.* **155,** 216–224 (2000).
21. K. B. Greenwood, G. M. Sarjeant, K. R. Poeppelmeier, P. A. Salvador, T. O. Mason, B. Dabrowski, K. Rogacki, and Z. Chen, *Chem. Mater.* **7,** 1355–1360 (1995).
22. K. D. Otzschi, K. R. Poeppelmeier, P. A. S alvador, T. O. Mason, H. Zhang, and L. D. Marks, *J. Am. Chem. Soc.* **118,** 8951–8952 (1996).
23. M. H. Kane, T. O. Mason, W. Sinkler, L. D. Marks, K. D. Otzschi, D. Ko, and K. R. Poeppelmeier, *J. Solid State Chem.* **148,** 3–15 (1999).